surfaces

MDPI

Article

Characterization of Mechanochemical Modification of Porous Silicon with Arginine

Jacklyn A. DiPietro and Kurt W. Kolasinski *

Department of Chemistry, West Chester University, West Chester, PA 19383, USA; JD915208@wcupa.edu
* Correspondence: kkolasinski@wcupa.edu; Tel.: +1-610-436-2968

Abstract: Mechanochemistry initiated the reaction of hydrogen-terminated porous silicon (H/por-Si) powder with arginine. Samples were analyzed using Fourier-transform infrared spectroscopy (FTIR), dynamic light scattering (DLS), zeta potential, scanning electron microscopy (SEM), and photoluminescence (PL) spectroscopy. Arginine, which was physisorbed onto the surface of por-Si, blue-shifted the peak PL intensity from ~630 nm for the H/por-Si to ~565 nm for arginine-coated por-Si. Grinding for 4 h reduced >80% of the initially 2–45 µm particles to <500 nm, but was observed to quench the PL. With appropriate rinsing and centrifugation, particles in the 100 nm range were isolated. Rinsing ground powder with water was required to remove the unreacted arginine. Without rinsing, excess arginine induced the aggregation of passivated particles. However, water reacted with the freshly ground por-Si powder producing H_2. A zeta potential of +42 mV was measured for arginine-terminated por-Si particles dispersed in deionized water. This positive value was consistent with termination such that NH_2 groups extended away from the surface. Furthermore, this result was confirmed by FTIR spectra, which suggested that arginine was bound to silicon through the formation of a covalent Si–O bond.

Keywords: passivation; chemisorption; porous silicon; arginine; surface modification; mechanochemistry; photoluminescence; zeta potential

check for updates

Citation: DiPietro, J.A.; Kolasinski, K.W. Characterization of Mechanochemical Modification of Porous Silicon with Arginine. *Surfaces* **2022**, *5*, 143–154. https://doi.org/10.3390/surfaces5010007

Academic Editor: Gaetano Granozzi

Received: 2 December 2021
Accepted: 20 January 2022
Published: 1 February 2022

Publisher's Note: MDPI stays neutral with regard to jurisdictional claims in published maps and institutional affiliations.

Copyright: © 2022 by the authors. Licensee MDPI, Basel, Switzerland. This article is an open access article distributed under the terms and conditions of the Creative Commons Attribution (CC BY) license (https://creativecommons.org/licenses/by/4.0/).

1. Introduction

The versatile chemical and physical properties of porous silicon (por-Si), including its biocompatibility, allow for applications in sensors [1], energy storage [2,3], and biomedicine [4]. Porous silicon can be formed through a variety of different methods, including regenerative electroless etching (ReEtching) [5], stain etching [6], and metal-assisted catalytic etching (MACE) [7]. Electroless production of por-Si possesses the distinct advantage of the ability to etch Si particles of arbitrary shape and size, in particular, it can etch Si powders irrespective of doping type and level [8].

The visible photoluminescence (PL) of mesoporous silicon arises from an interplay of quantum confinement and surface passivation effects [9]. Its optical properties facilitate applications in biological imaging [10] excited with one or two photons [11,12], in theranostics [13] and photodynamic therapy [14]. In addition, porous silicon has many advantages in pharmaceuticals and drug delivery, as its pore size, pore volume, and specific surface area are all tunable, which allow for the loading of a wide variety of organic species, such as small molecule drugs [15], RNA [16], insulin [17], and peptides [18]. The surface chemistry of Si is extremely versatile. It can be hydrophobic or hydrophilic and even coated with antigens [19]. However, the biosafety of silicon is critical for its potential use in medicine [20]. Flat silicon is already prevalent in medical devices, such as implants and pacemakers, but is considered to be bioincompatible [21]. In comparison, nanostructured porous silicon can be resorbed by the body and decomposed into silicic acid, a bioavailable form of silicon that can be eliminated naturally [20]. Therefore, the relative nontoxicity of nanostructured porous silicon in vivo coupled with its photoluminescence and the ability

to load organic molecules onto its surface make the use of silicon nanoparticles viable in the fields of pharmaceuticals, drug delivery, and biomedical imaging.

A promising but underutilized technique for the attachment of organic molecules to porous silicon is the mechanochemical approach, i.e., grinding. Mechanochemistry is a solid-state approach to chemical synthesis, enabled by external mechanical forces. Grinding helps in initiating and stimulating chemical reactions between solids or between solids and liquids. This method aims to reduce or even avoid the use of solvents in the synthesis process and is often referred to as a method of "green chemistry" [22].

Conventional methods of reaction between organic molecules and silicon generally involve multi-step reactions that proceed by refluxing in the presence of large quantities of solvents that may themselves be toxic. Grinding, unlike refluxing, is easily scaled to large volumes, and represents a more energy and time efficient, lower waste generating, simpler synthetic method. Furthermore, the reaction remains inside an enclosed environment, whose parameters, such as time of grind, media size, and media-to-sample ratio can easily be adjusted to obtain the desired product [23]. On the other hand, mechanochemistry may also introduce unwanted non-radiative defects to the Si powder. The continuous impact of alumina grinding media on nanostructured silicon may induce stress, fractures, surface defects, oxidation, and radical formation [24]. Therefore, there is a need to elucidate the way grinding impacts the chemical properties of porous silicon and determine the response of material properties, such as particle size and PL to grinding parameters.

To more fully exploit por-Si for applications in drug delivery, antimicrobial activity, and biomedical imaging, it is crucial to find safe, affordable, and effective methods for the preparation and synthesis of organic molecules bound to porous silicon. In this study, we focus on the way grinding affects the size, photoluminescence, and chemical structure of the resulting silicon nanoparticles. We present strong evidence that grinding produces surface free radicals associated with Si dangling bonds. Furthermore, we demonstrate for the first time that mechanochemistry can be used to initiate a reaction between arginine—a water soluble molecule that is unsuitable for conventional hydrosilylation—and por-Si to generate surface-modified samples with a positive zeta potential. Physisorbed arginine strongly blueshifts PL. However, nonradiative traps generated during grinding reduce the PL intensity.

2. Materials and Methods

2.1. Mechanochemical Synthesis

Metallurgical grade Si powder (MG-Si) was provided by Elkem Materials Inc. (Oslo, Norway, Silgrain HQ, 99.6% purity, 800 μm particles). This was ground and sieved to select < 45 μm particles. The powder was washed by sonication for 60 min in a mixture of 3% H_2O_2 (all of the chemicals are from Fisher Scientific, ACS reagent, Pittsburgh, PA, USA unless otherwise noted) and deionized water. Roughly, a 150 mL solution per 10 g of Si powder was used for washing. Filtration isolated particles were in the size range of 2–45 μm. Grinding, both to produce the initial Si powder and for mechanochemistry, was performed with 0.25-in or 1-in alumina cylinders (Burundum grinding media and grinding jar from E.R. Advanced Ceramics Inc., East Palestine, OH, USA).

ReEtched porous silicon powders were produced as described in detail in other research works [25]. Approximately 0.15 g of V_2O_5 (Fisher Scientific certified) was dissolved in 20 mL of concentrated HF (Acros Organics, 49% ACS reagent). In a separate beaker, approximately 1 g of Si was dispersed in 20 mL of acetic acid (Fisher Scientific, ACS reagent). Both beakers were placed in a thermally insulated ice/water bath to maintain a temperature close to 0 °C during etching. The contents of the HF/V_2O_5-containing beaker were added to the Si-containing beaker. While the mixture was agitated with a Teflon-coated magnetic stir bar, 3.27 mL of H_2O_2 (Fisher Scientific, 30% certified ACS or proportionally less Acros Organics, 35% ACS reagent) was injected over 85 min (molar ratio H_2O_2:Si = 0.9:1) using a KD Scientific, Legato 100 syringe pump. The etchant was decanted 5 min after the end of H_2O_2 injection. The etched Si was filtered in a polypropylene Büchner funnel using

2.5 μm Whatman filter paper. The etched powder was rinsed with copious 0.2 M HCl(aq), a minimal amount of ethanol, and then wetted with pentane. When Si appeared nominally dry, the filter top was placed in a vacuum oven at ~50 °C and the oven was evacuated with an alumina-trapped mechanical pump. After at least several hours, Si was removed from the oven and weighed, then placed in a sealed glass vial.

To perform mechanochemistry, grinding was performed using a 1:1 ratio of Si powder to arginine (approximately 0.2 g each). The size 000 Roalox grinding jar was more stable and ground more efficiently with the 1-inch media. To reduce oxidation, prior to grinding, all of the reagents, including grinding media and the grinding jar, were dried in a vacuum oven overnight at 50 °C. In addition, the jar was purged with argon gas prior to the addition of reagents, and ~2 mL pentane was added before sealing. The grinding procedure involved filling the cylindrical jar with grinding media and reagents and rotating the jar around its longitudinal axis.

Periodically during mechanochemistry, a sample was removed from the vessel and drop casted onto a Si wafer, adhering to a carbon adhesive disk (SPI Supplies, West Chester, PA, USA) affixed to a Si wafer or retained as powder for analysis. Drop casting was performed by adding enough ethanol to form a film over the wafer, coating it with the powder, and allowing for the evaporation of ethanol. After each sample was taken, ~2 mL pentane was added before grinding was continued.

After mechanochemistry, the powders were collected from the grinding jar and separated from the alumina media by rinsing. Several solvents including water, pentane, and ethanol were tested for their ability to avoid oxidation and overall rinsing effectiveness. In the separation process, ground powders dispersed in ethanol or water were spun down with a centrifuge (Eppendorf Model 5810 R, Hamburg, Germany) at 1800–2400 relative centrifugal force (rcf) for 15–30 min until the powder sedimented.

2.2. Dynamic Light Scattering

To determine the particle size distribution and zeta potential of the powders, a Zetasizer Pro (Malvern Panalytic, Malvern, UK) was used to perform dynamic light scattering (DLS). The location in the jar from which the sample was taken may have affected the size distribution determined by DLS. For example, powder collected from the lid of the grinding jar versus powder collected from the bottom may have different sizes. Therefore, sampling was taken from multiple locations in the jar and mixed prior to characterization. Si particles were dispersed by sonication for 1 min in ethanol prior to size determination. Scanning electron microscopy (FEI Quanta 400 SEM, Hillsboro, OR, USA) was used to characterize the particle shape.

2.3. Photoluminescence

A Cary Eclipse fluorescence spectrometer (Agilent Technologies, Inc., Santa Clara, CA, USA) with a solid sample holder attachment was used to analyze the photoluminescence of the nanoparticles. The excitation wavelength was set to 340 nm, with the excitation slit set to 5 nm and the emission slit set to 10 nm, unless noted otherwise. For measurement, a Si wafer with drop cast powder or powder affixed to a carbon adhesive disk was placed on the solid sample mount inside the fluorimeter.

2.4. Infrared Spectroscopy

A Nicolet iS50 Fourier-transform infrared spectrometer (FTIR) (Thermo Fisher Inc., Waltham, MA, USA) equipped with a diffuse reflectance (DR) or attenuated total reflectance (ATR) attachment was used to collect IR spectra and confirm the chemical termination of silicon surfaces. Spectra were acquired with 4 or 8 cm^{-1} resolution averaging over 64 or 128 scans. IR spectra were simulated using Spartan Quantum Chemical Software (Wavefunction Inc., Irvine, CA, USA) [26]. Calculations were performed on a $Si_{32}H_{36}$ cluster using the density functional theory (DFT) with a 6–31G* basis set and a ωB97X-D exchange functional. The Si cluster exposed a dihydride-terminated Si(001) surface with

one adsorbed H atom replaced by a molecular fragment originating from arginine bound at either end of the molecule. All of the Si atoms at the edge of the cluster are terminated with H atoms that are assigned the same mass as a Si atom. This engenders the tetrahedral coordination of all Si atoms without introducing spurious dipole moments. Moreover, it decouples the vibrational motion of the H atoms terminating the Si(001) surface from the heavy H atoms in order that spurious vibrational modes are not introduced.

3. Results

3.1. Rinsing and Separation

In a typical rinsing cycle, 0.5 g ground Si is removed from the grinding jar with 150 mL ethanol or water. This is distributed evenly into six 50-mL centrifuge tubes, capped after piercing a hole in the cap, and centrifuged at 2400 rcf to pellet the powder. To wash arginine from a pelleted sample, typically three rinsing cycles are performed. First, the pellet is dispersed in 25 mL water and centrifuged. Then, the pellet is dispersed two additional times in 10 mL water and centrifuged. Thereafter, the sample is ready for characterization with DLS or for zeta potential measurement. If a dry sample is required, the sample is dispersed in 10 mL of ethanol and centrifuged prior to drying.

When water was used to rinse ground Si powder from the grinding jar, significant bubbling was observed from the dispersion. This was observed for grinding both with and without arginine. Sufficient gas was evolved to increase the pressure within a centrifuge tube to the point of rupture if a hole was not pierced in the cap. We confirmed that the gas evolved was H_2 by detection with an electronic leak detector (model 28500 Restek Corporation, Bellefonte, PA, USA).

Ethanol was highly effective in the rinsing and separation process. Significant bubbling was not observed and no H_2 gas was detected for grinding both with and without arginine. Therefore, ethanol should be used in the rinsing and separation process if oxidation is to be avoided. However, arginine is not soluble in ethanol. Therefore, if unreacted, arginine is to be removed and water must be used. In this case, pentane was not found to be an efficient rinsing agent.

3.2. Particle Size and Zeta Potential

Dry ReEtched por-Si powder is hydrophobic and cannot be dispersed in water to measure the zeta potential of the H-terminated surface in the absence of surfactants. Grinds of pure porous powder and por-Si + arginine were performed with samples taken periodically. Powder that was ground with arginine acted as "sticky" and aggregated readily unless excess arginine was removed. Therefore, the particle size of ground washed por-Si was consistently smaller than the mixture in the presence of excess arginine. Sonication for 1 min dispersed the powders into the solution and separated these aggregates to some degree prior to measurement. However, repeatedly performing the DLS experiments one after another indicated that aggregation in the presence of arginine was occurring on the timescale of data acquisition.

The particle size distribution obtained from grinding was initially extremely broad. Settling, rinsing, and repeated steps of centrifugation were used to isolate particles of different size distributions in the supernatant or the pellet. After 4 h of grinding while still dispersed in ethanol, essentially all of the particles exhibited sizes below 4 μm with ~80% of particles exhibiting sizes below 500 nm. When redispersed ultrasonically in ethanol and then centrifuged at 2400 rcf for 30 min, the supernatant exhibited a Z-average particle size of 230 nm with PDI = 0.107. After three cycles of rinsing with water, centrifuging, and redispersing, the supernatant was characterized by a Z-average of 113 nm with PDI = 0.164. As shown in Figure 1, SEM analysis confirmed that Si particles were initially quite angular with sharp edges and smooth surfaces. After etching and grinding, the particles were significantly more irregular with additional rounded edges and a good amount of embedded material that made the surfaces rougher.

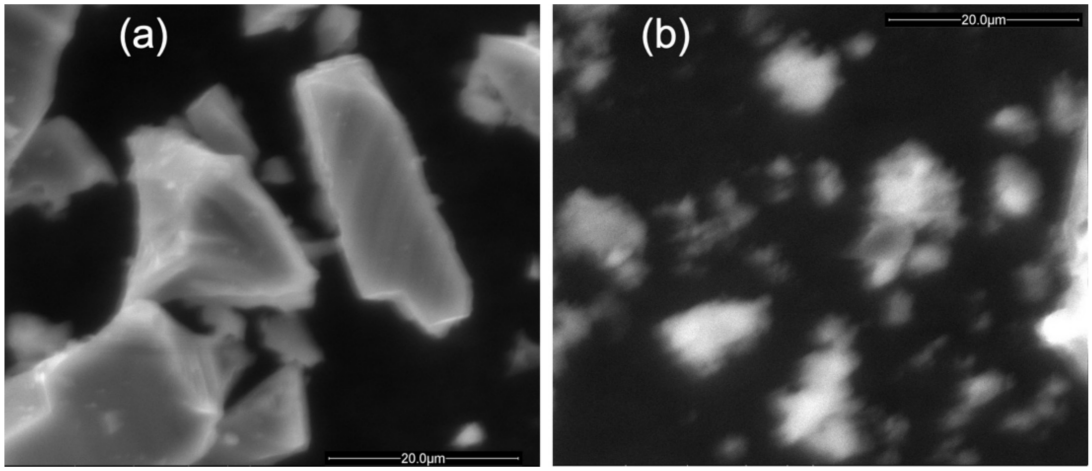


Figure 1. (**a**) An SEM micrograph of the starting material, which was unetched, washed with metallurgical grade Si powder. (**b**) Si particles after etching and grinding without arginine.

As shown in Figure 2, the surface of arginine-modified por-Si was positively charged with a mean zeta potential of +42 mV. This result is quite interesting since, as we shall see below, significant oxidation of por-Si occurred during mechanochemistry. Yakin et al. [27] have reported that porous *silica* nanoparticles have a *negative* zeta potential in aqueous solutions near neutral pH. The positive zeta potential that we observed at neutral pH strongly supports the conclusion that the surfaces created by mechanochemical modification with arginine were bound in a way that the NH_2 end of the molecule was pointing away from the surface. Evidently, the observed oxidation to form Si–O bonds is not linked to the formation of an appreciable amount of surface silanol groups.

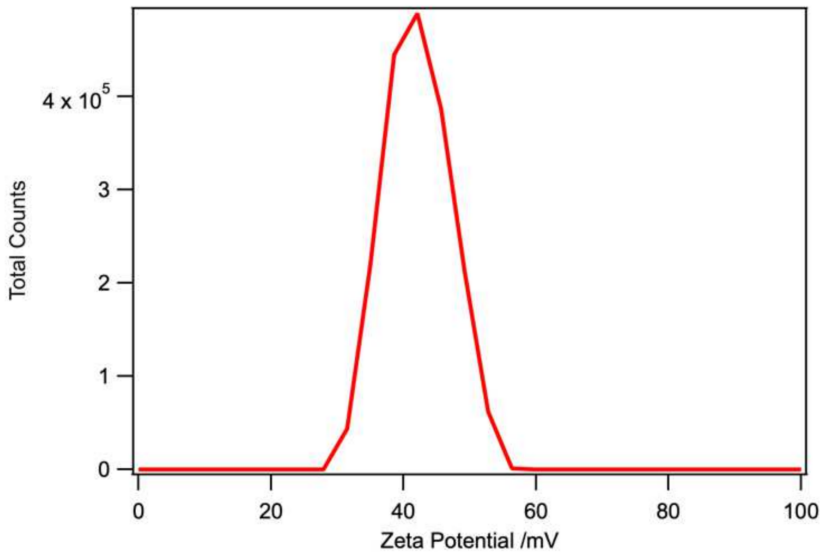


Figure 2. Zeta potential measured for por-Si coated with arginine after grinding for 4 h from a sample with a Z-average particle size of 230 nm.

3.3. Photoluminescence

Without grinding, the photoluminescence of ReEtched por-Si powder exhibited strong red-orange emission. The PL spectrum displayed in Figure 3 was fitted to a skew Gaussian [25] with an intensity of A = 59 a.u., a peak wavelength of λ_{max} = 629 nm, and a width of σ = 154 nm. Grinding without arginine led to virtually complete quenching of the PL (not shown). Coating the por-Si with arginine (melting point = 244 °C) by heating a mixture of arginine + por-Si to 250 °C under flowing N_2 significantly blue-shifted the peak

to 565 nm with a slight reduction in intensity A = 39 a.u., while making the peak narrower σ = 137 nm. Grinding for 2 h or 4 h in the presence of arginine did little to the peak position or width (λ_{max} ~ 555 nm, σ ~ 123 nm). However, while grinding for 2 h increased the PL intensity, A = 111 a.u., grinding for 4 h led to a substantial reduction in intensity, A = 19 a.u. By rinsing to remove any arginine that was not covalently bound to the surface, the peak position did not change substantially, λ_{max} ~ 568 nm, whereas the PL intensity was greatly reduced, A = 3 a.u. and the peak broadened somewhat (σ = 144 nm). This indicated that physisorbed arginine was capable of significantly modifying the PL response of por-Si. However, the non-radiative traps induced by prolonged grinding, particularly after rinsing to remove physisorbed arginine that had not become covalently bound, were detrimental to the PL intensity. The blueshift in the presence of arginine is reproducible from sample to sample. Similarly, the almost complete quenching after prolonged grinding and rinsing away physisorbed arginine was consistently observed. However, the absolute intensity fluctuated from sample to sample, and we have not tried to quantify trends in the intensity.

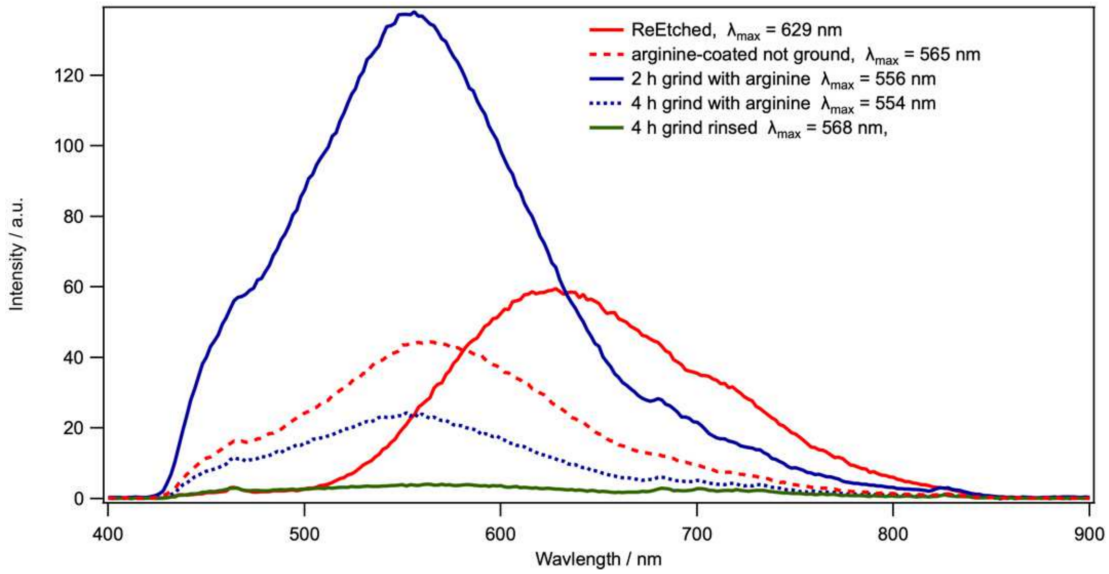


Figure 3. Comparison of the photoluminescence of por-Si powder before grinding (red curves, both as-etched and coated with arginine), por-Si after grinding 2 h or 4 h with arginine (blue curves), and por-Si powder ground with arginine coated with covalently bound arginine, but after rinsing away physisorbed arginine (green curve).

3.4. FTIR

To confirm the covalent attachment of arginine to the por-Si surface, we used the spectroscopic analysis with FTIR combined with quantum chemical calculations to support the assignment and interpretation of the spectra. As shown in Figure 4 and consistent with the previous analysis [25,28], the as-etched surface of ReEtched por-Si was primarily covered with a combination of SiH and SiH_2 species adsorbed in sites similar to Si(001) and Si(110) planes. The presence of adsorbed SiH and SiH_2 moieties was confirmed by the broad feature in the 2070–2100 cm^{-1} range, which peaked at 2085 cm^{-1} and was associated with Si–H stretching modes. The sharp 900 cm^{-1} feature was assigned to the SiH_2 scissors mode, while a broader low wavenumber peak consisted of overlapping features at 616, 655, and 715 cm^{-1} associated with a variety of SiH and SiH_2 wags. These assignments were consistent with previous reports, as well as a comparison of the vibrational spectrum calculated for a fully H-terminated $Si_{32}H_{36}$ cluster using DFT. Due to the assumption of harmonic behavior, it is well-known that these calculations tend to overestimate the wavenumber of vibrations. A redshift of approximately 75–85 cm^{-1} brought the calculated spectra into agreement with the observed spectra on the H-terminated surface. The smaller peaks associated with the carbonyl stretch at 1705 cm^{-1} and C–H stretches at 2850 and

2920 cm^{-1} were assigned to acetic acid fragments bound through an Si–O linkage. Acetic acid is used as a surfactant and solvent during ReEtching. The lack of a feature in the O–H stretching region above 3000 cm^{-1} confirmed the formation of an Si–O linkage.

After grinding without arginine, the Si–H region was broadened due to the disorder and insertion of O atoms into the Si–Si back bonds under Si–H groups, which is known to blueshift the peaks. The SiH2 scissors peak was also broadened. The peak near 1040 cm^{-1} was associated with Si–O stretches and confirmed partial oxidation of the sample. After grinding with arginine for 4 h followed by rinsing with water and drying, the FTIR spectrum of por-Si exhibited significant modification. The Si–H stretching region decreased in intensity while broadening in width. The loss of intensity was consistent with the removal of adsorbed H atoms through substitution by other adsorbates. Broadening indicated greater inhomogeneity in adsorption sites introduced by disorder, defects, and possibly the introduction of Si(111) facets by mechanical cleavage during grinding, which results in particle size reduction. Whereas Si(001) and Si(110) facets are the most likely to be produced by etching, Si(110) and Si(111) facets are the most likely to be produced by cleavage [29]. Moreover, significant oxidation of por-Si was observed as indicated by the large peak at 1038 cm^{-1}.

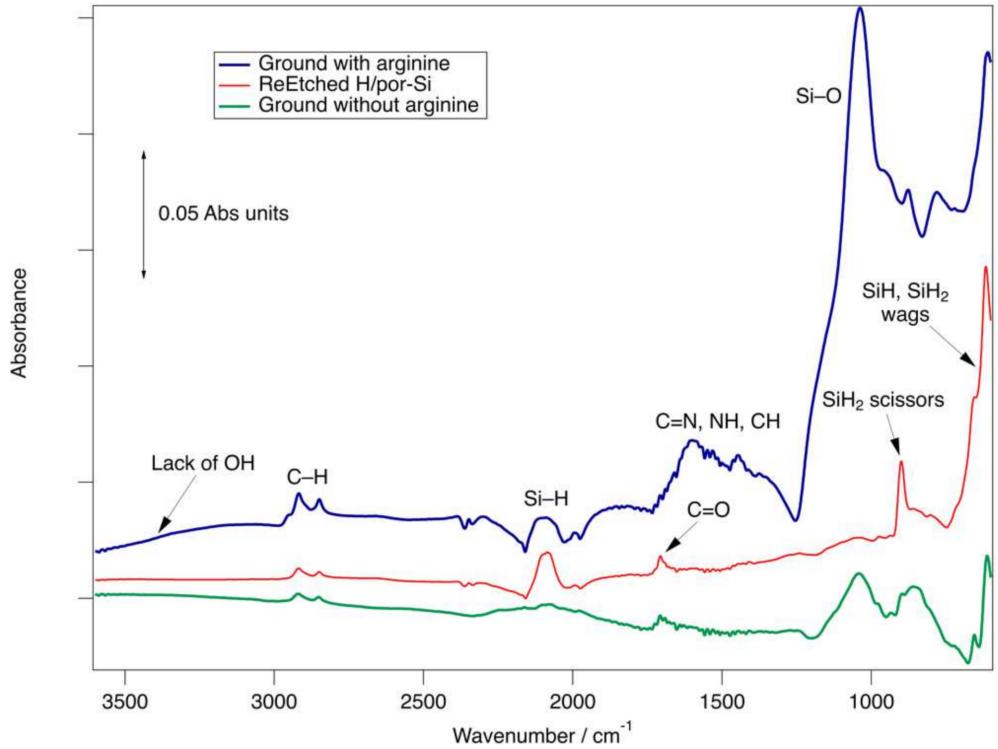


Figure 4. FTIR spectrum from 1200–3600 cm^{-1}. The red spectrum in the middle belongs to the as-etched por-Si. The green spectrum at the bottom belongs to por-Si ground for 4 h without arginine. The upper blue spectrum is obtained after a 4-h grind of por-Si with arginine. The sample ground with arginine was rinsed to remove excess and physisorbed arginine. CO_2 and H_2O features are due to incomplete purging of atmospheric gas.

To interpret the FTIR spectra, we simulated the vibrational spectra for $Si_{32}H_{36}$ clusters from which one H atom was removed from the cluster and one H atom was removed from arginine, NH_2RCOOH, to produce an adsorbate that was bound through the N end, Si–NHRCOOH(a) or O end, Si–$OOCRNH_2$(a). Here, we refer to the surface-bound end of the molecule as the α end and the end of the adsorbed molecule that points away from the surface as the ω end. The resulting structures are shown in Figure 5.



(**a**) Si–N linkage (**b**) Si–O linkage

Figure 5. (**a**) Optimized geometry of arginine bound to a Si_{32} cluster with an H-terminated Si(001) surface through an Si–N linkage created by attachment through the $–NH_2$ group with loss of H_2. This geometry creates an adsorbate with a carboxyl group –COOH at its ω terminus. (**b**) Optimized geometry of arginine bound to a Si_{32} cluster with an H-terminated Si(001) surface through an Si–O linkage created by attachment through the –OH group with loss of H_2. This geometry creates an adsorbate with an amine group $–NH_2$ at its ω terminus.

The simulated FTIR spectra resulting from these calculations are shown in Figure 6. Of note, these spectra were simulated for a single isolated adsorbate. Therefore, the broadening due to lateral interactions and adsorption site inhomogeneities was absent. The most salient features to emphasize are that the N–H stretches (3400–3500 cm^{-1}) are extremely weak, while the C=N stretch (1683 or 1641 cm^{-1}), NH_2 scissors (1582 cm^{-1}), and NH or OH wag (1404 or 1420 cm^{-1}) are quite strong in the Si–O or Si–N configurations, respectively. The most distinctive differences are that the Si–N configuration with COOH ω end should exhibit a strong O–H stretch at 3276 cm^{-1} and a strong and distinct C=O stretch (1804 cm^{-1}). In contrast, the Si–O configuration with an NH_2 ω end is missing the O–H related feature. In addition, the C=O stretch at 1723 cm^{-1} is not only significantly weaker, but also less distinct since it is not well-resolved from the C=N stretch. By comparison of the simulated spectra with the full spectrum of Figure 4, we concluded that mechanochemistry fostered the attachment of arginine to produce an Si–O linkage and NH_2 terminus.

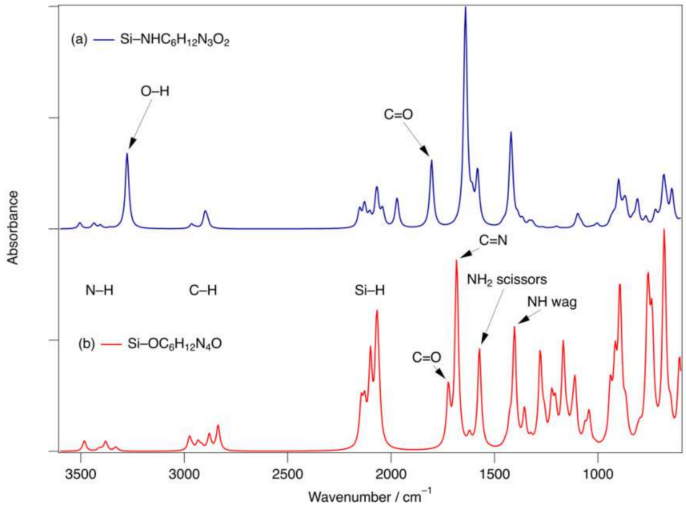


Figure 6. (**a**) Simulated FTIR spectrum of Si–N bound arginine. Note the prominent stretch of free OH at 3276 cm^{-1} and the distinct C=O carbonyl stretch at 1804 cm^{-1}. (**b**) Simulated FTIR spectrum of Si–O bound arginine. Note the more congested region from 1400–1700 cm^{-1}.

4. Discussion

Mechanochemistry reduced the mean particle size of por-Si powder. This occurs by cleavage of the polycrystalline powder, which exposes Si surface atoms with dangling bonds. The presence of these dangling bonds initiated further chemistry. First, we observed this when water was used to rinse ground por-Si from the grinding jar, which generated H_2 gas. One might consider the oxidative displacement of H_2 by water to produce H_2 following the reaction:

$$\mathrm{SiH(a) + H_2O(l) \rightarrow SiOH(a) + H_2(g).} \quad (1)$$

However, the H-terminated surface is stable and requires activation in the form of heat [30,31], light [32,33], bias [34], strong oxidant [35], microwave [36,37] or radical initiator [38] as has been reviewed recently [39]. Therefore, Rxn. (1) does not occur at an appreciable rate at room temperature. In the absence of any other form of activation, it must be the presence of highly reactive dangling bonds that initiates reactivity to produce H_2. Dissociative adsorption on two dangling bond sites (on a single Si atom or two adjacent sites),

$$\mathrm{2Si\bullet(a) + H_2O(l) \rightarrow SiH(a) + SiOH(a),} \quad (2)$$

does not lead to H_2 desorption. Therefore, it must be followed by a second step involving a condensation reaction of neighboring silanol groups, as follows:

$$\mathrm{2SiOH(a) \rightarrow 2SiO(a) + H_2(g).} \quad (3)$$

Condensation of Si–OH to Si–O–Si bridges and substoichiometric SiO_{2-x} nuclei has been proposed previously to explain the initial stages of oxidation of Si by water [40,41].

FTIR spectra and the positive zeta potential suggested the attachment of arginine by the formation of an Si–O bond to form Si–$OOCRNH_2$(a). In analogy to Rxn. (2), a plausible reaction to form this species is as follows:

$$\mathrm{2Si\bullet(a) + HOOCRNH_2(s) \rightarrow SiH(a) + Si\text{-}OOCRNH_2(a).} \quad (4)$$

The resulting adsorbate structure is shown in Figure 5b. Interestingly, the total energies calculated with DFT in the two configurations differ by an inconsequential 1 kJ mol^{-1}. Therefore, the prevalence of the NH_2-terminated species must result from the kinetically favored formation of the Si–O linkage compared to the Si–N linkage.

Prior to grinding, ReEtched por-Si exhibited a strong red-orange PL due to the good electronic passivation provided by the predominantly H-terminated surface. The requirement for two adjacent Si• sites or a diradical site may explain the strong quenching of PL upon grinding, as numerous isolated dangling bond sites will remain after the reaction with arginine. Dangling bonds will act as non-radiative traps. The addition of pentane during grinding did not prove effective in providing H atoms to terminate these sites, which may require the addition of a terminal alkene for this passivation step.

Physisorbed arginine shifted the PL intensity maximum from red orange (630 nm) to green (565 nm) with little loss of intensity. The origin of the blueshift is unclear. However, it is clear that physisorbed arginine was quite efficient at passivating non-radiative defects present on the surface. The peak position remained the same in the presence of covalently bound arginine. However, the greatly reduced PL intensity after rinsing to remove physisorbed arginine was ascribed to the uncovering of surface defects. Removal of physisorbed arginine caused non-radiative traps to no longer be passivated. As a result, finding methods to passivate these non-radiative traps is currently investigated.

5. Conclusions

In the present paper, we have shown that mechanochemistry can modify H-terminated porous Si with a covalently linked arginine fragment. The modified surface exhibits a positive zeta potential in neutral aqueous solution due to the NH_2 group at the ω end

of the adsorbate. Arginine is not suitable for hydrosilylation, which is commonly used to chemically modify H-terminated por-Si, due to its low solubility in nonpolar high-boiling point organic solvents. Herein, the demonstrated mechanochemical route should be generally applicable to other polar organic compounds and is easily scalable to large volumes. In future work, we will investigate (1) the dependence of photoluminescence fading by pursuing methods to passivate the non-radiative traps introduced by grinding, and (2) the dependence of PL intensity and peak wavelength shift on the presence of physisorbed molecules. Furthermore, we will investigate how passivation with arginine or other moieties affects the loading of molecules, e.g., pharmaceuticals, into porous silicon.

Author Contributions: Conceptualization, K.W.K.; methodology, K.W.K.; formal analysis, K.W.K. and J.A.D.; investigation, K.W.K. and J.A.D.; resources, K.W.K.; data curation, K.W.K.; writing—original draft preparation, J.A.D.; writing—review and editing, K.W.K. and J.A.D.; supervision, K.W.K.; project administration, K.W.K.; funding acquisition, K.W.K. All authors have read and agreed to the published version of the manuscript.

Funding: Supported by funding provided by the National Science Foundation award #1825331 and the Pennsylvania State System of Higher Education Technology Fee Program.

Institutional Review Board Statement: Not applicable.

Informed Consent Statement: Not applicable.

Data Availability Statement: The data presented in this study are available on request from the corresponding author.

Acknowledgments: We appreciate the support of Samantha L. Shumlas of the Center for Microanalysis and Imaging Research and Training (CMIRT) for her expert assistance with the collection and evaluation of SEM data.

Conflicts of Interest: The authors declare no conflict of interest.

References

1. Moretta, R.; De Stefano, L.; Terracciano, M.; Rea, I. Porous Silicon Optical Devices: Recent Advances in Biosensing Applications. *Sensors* **2021**, *21*, 1336. [CrossRef] [PubMed]
2. Armstrong, M.J.; O'Dwyer, C.; Macklin, W.J.; Holmes, J.D. Evaluating the performance of nanostructured materials as lithium-ion battery electrodes. *Nano Res.* **2014**, *7*, 1–62. [CrossRef]
3. Dai, F.; Yi, R.; Yang, H.; Zhao, Y.; Luo, L.; Gordin, M.L.; Sohn, H.; Chen, S.; Wang, C.; Zhang, S.; et al. Minimized Volume Expansion in Hierarchical Porous Silicon upon Lithiation. *ACS Appl. Mater. Interfaces* **2019**, *11*, 13257–13263. [CrossRef] [PubMed]
4. Alhmoud, H.; Brodoceanu, D.; Elnathan, R.; Kraus, T.; Voelcker, N.H. A MACEing silicon: Towards single-step etching of defined porous nanostructures for biomedicine. *Prog. Mater. Sci.* **2021**, *116*, 100636. [CrossRef]
5. Kolasinski, K.W.; Gimbar, N.J.; Yu, H.; Aindow, M.; Mäkilä, E.; Salonen, J. Regenerative Electroless Etching of Silicon. *Angew. Chem. Int. Ed. Engl.* **2017**, *56*, 624–627. [CrossRef]
6. Kolasinski, K.W. Porous silicon formation by stain etching. In *Handbook of Porous Silicon*, 2nd ed.; Canham, L.T., Ed.; Springer: Berlin/Heidelberg, Germany, 2017; pp. 1–21. [CrossRef]
7. Huo, C.; Wang, J.; Fu, H.; Li, X.; Yang, Y.; Wang, H.; Mateen, A.; Farid, G.; Peng, K.-Q. Metal-Assisted Chemical Etching of Silicon in Oxidizing HF Solutions: Origin, Mechanism, Development, and Black Silicon Solar Cell Application. *Adv. Func. Mater.* **2020**, *30*, 2005744. [CrossRef]
8. Kolasinski, K.W. Metal-Assisted Catalytic Etching (MACE) for Nanofabrication of Semiconductor Powders. *Micromachines* **2021**, *12*, 776. [CrossRef]
9. Canham, L. Introductory lecture: Origins and applications of efficient visible photoluminescence from silicon-based nanostructures. *Faraday Discuss.* **2020**, *222*, 10–81. [CrossRef]
10. Smith, B.R.; Gambhir, S.S. Nanomaterials for In Vivo Imaging. *Chem. Rev.* **2017**, *117*, 901–986. [CrossRef]
11. Furey, B.J.; Silbaugh, D.A.; Yu, Y.; Guillaussier, A.C.; Estrada, A.D.; Stevens, C.; Maynard, J.A.; Korgel, B.A.; Downer, M.C. Measurement of Two-Photon Absorption of Silicon Nanocrystals in Colloidal Suspension for Bio-Imaging Applications. *Phys. Status Solidi (b)* **2018**, *255*, 1700501. [CrossRef]
12. Kim, D.; Kang, J.; Wang, T.; Ryu, H.G.; Zuidema, J.M.; Joo, J.; Kim, M.; Huh, Y.; Jung, J.; Ahn, K.H.; et al. Two-Photon In Vivo Imaging with Porous Silicon Nanoparticles. *Adv. Mater.* **2017**, *29*, 1703309. [CrossRef]
13. Li, W.; Liu, Z.; Fontana, F.; Ding, Y.; Liu, D.; Hirvonen, J.T.; Santos, H.A. Tailoring Porous Silicon for Biomedical Applications: From Drug Delivery to Cancer Immunotherapy. *Adv. Mater.* **2018**, *30*, 1703740. [CrossRef]

14. Kumeria, T.; McInnes, S.J.P.; Maher, S.; Santos, A. Porous silicon for drug delivery applications and theranostics: Recent advances, critical review and perspectives. *Expert Opin. Drug Deliv.* **2017**, *14*, 1407–1422. [CrossRef]
15. Mäkilä, E.; Kivelä, H.; Shrestha, N.; Correia, A.; Kaasalainen, M.; Kukk, E.; Hirvonen, J.; Santos, H.A.; Salonen, J. Influence of Surface Chemistry on Ibuprofen Adsorption and Confinement in Mesoporous Silicon Microparticles. *Langmuir* **2016**, *32*, 13020–13029. [CrossRef]
16. Turner, C.T.; Hasanzadeh Kafshgari, M.; Melville, E.; Delalat, B.; Harding, F.; Mäkilä, E.; Salonen, J.J.; Cowin, A.J.; Voelcker, N.H. Delivery of Flightless I siRNA from Porous Silicon Nanoparticles Improves Wound Healing in Mice. *ACS Biomater. Sci. Eng.* **2016**, *2*, 2339–2346. [CrossRef]
17. Martins, J.P.; D'Auria, R.; Liu, D.; Fontana, F.; Ferreira, M.P.A.; Correia, A.; Kemell, M.; Moslova, K.; Mäkilä, E.; Salonen, J.; et al. Engineered Multifunctional Albumin-Decorated Porous Silicon Nanoparticles for FcRn Translocation of Insulin. *Small* **2018**, *14*, 1800462. [CrossRef]
18. Jin, Y.S.; Kim, D.; Roh, H.; Kim, S.; Hussain, S.; Kang, J.Y.; Pack, C.G.; Kim, J.K.; Myung, S.J.; Ruoslahti, E.; et al. Tracking the Fate of Porous Silicon Nanoparticles Delivering a Peptide Payload by Intrinsic Photoluminescence Lifetime. *Adv. Mater.* **2018**, *30*, 1802878. [CrossRef]
19. Cifuentes-Rius, A.; Ivask, A.; Sporleder, E.; Kaur, I.; Assan, Y.; Rao, S.; Warther, D.; Prestidge, C.A.; Durand, J.-O.; Voelcker, N.H. Dual-Action Cancer Therapy with Targeted Porous Silicon Nanovectors. *Small* **2017**, *13*, 1701201. [CrossRef]
20. Henstock, J.R.; Canham, L.T.; Anderson, S.I. Silicon: The evolution of its use in biomaterials. *Acta Biomater.* **2015**, *11*, 17–26. [CrossRef]
21. Low, S.; Voelcker, N.; Canham, L.; Williams, K. The biocompatibility of porous silicon in tissues of the eye. *Biomaterials* **2009**, *30*, 2873–2880. [CrossRef] [PubMed]
22. Szczęśniak, B.; Borysiuk, S.; Choma, J.; Jaroniec, M. Mechanochemical synthesis of highly porous materials. *Mater. Horiz.* **2020**, *7*, 1457–1473. [CrossRef]
23. Do, J.-L.; Friščić, T. Mechanochemistry: A Force of Synthesis. *ACS Cent. Sci.* **2016**, *3*, 13–19. [CrossRef]
24. Russo, L.; Colangelo, F.; Cioffi, R.; Rea, I.; Stefano, L.D. A Mechanochemical Approach to Porous Silicon Nanoparticles Fabrication. *Materials* **2011**, *4*, 1023–1033. [CrossRef]
25. Kolasinski, K.W.; Swanson, J.D.; Roe, B.; Lee, T. Response of Photoluminescence of H-Terminated and Hydrosilylated Porous Si Powders to Rinsing and Temperature. *Surfaces* **2020**, *3*, 366–380. [CrossRef]
26. Shao, Y.; Gan, Z.; Epifanovsky, E.; Gilbert, A.T.B.; Wormit, M.; Kussmann, J.; Lange, A.W.; Behn, A.; Deng, J.; Feng, X.; et al. Advances in molecular quantum chemistry contained in the Q-Chem 4 program package. *Mol. Phys.* **2015**, *113*, 184–215. [CrossRef]
27. Yakin, F.E.; Barisik, M.; Sen, T. Pore Size and Porosity Dependent Zeta Potentials of Mesoporous Silica Nanoparticles. *J. Phys. Chem. C* **2020**, *124*, 19579–19587. [CrossRef]
28. Kolasinski, K.W.; Hartline, J.D.; Kelly, B.T.; Yadlovskiy, J. Dynamics of Porous Silicon Formation by Etching in HF + V_2O_5 Solutions. *Mol. Phys.* **2010**, *108*, 1033–1043. [CrossRef]
29. Kolasinski, K.W.; Unger, B.A.; Ernst, A.T.; Aindow, M. Crystallographically Determined Etching and Its Relevance to the Metal-Assisted Catalytic Etching (MACE) of Silicon Powders. *Front. Chem.* **2019**, *6*, 651. [CrossRef]
30. Jarvis, K.L.; Barnes, T.J.; Prestidge, C.A. Surface chemistry of porous silicon and implications for drug encapsulation and delivery applications. *Adv. Colloid Interface Sci.* **2012**, *175*, 25–38. [CrossRef] [PubMed]
31. Peng, W.; Rupich, S.M.; Shafiq, N.; Gartstein, Y.N.; Malko, A.V.; Chabal, Y.J. Silicon Surface Modification and Characterization for Emergent Photovoltaic Applications Based on Energy Transfer. *Chem. Rev.* **2015**, *115*, 12764–12796. [CrossRef] [PubMed]
32. Escorihuela, J.; Zuilhof, H. Rapid Surface Functionalization of Hydrogen-Terminated Silicon by Alkyl Silanols. *J. Am. Chem. Soc.* **2017**, *139*, 5870–5876. [CrossRef]
33. Kolasinski, K.W. Silicon surface photochemistry. In *Encyclopedia of Interfacial Chemistry: Surface Science and Electrochemistry*; Wandelt, K., Ed.; Elsevier: Oxford, UK, 2018; Volume 2, pp. 611–620.
34. Aswal, D.K.; Koiry, S.P.; Jousselme, B.; Gupta, S.K.; Palacin, S.; Yakhmi, J.V. Hybrid molecule-on-silicon nanoelectronics: Electrochemical processes for grafting and printing of monolayers. *Phys. E Low-Dimens. Syst. Nanostructures* **2009**, *41*, 325–344. [CrossRef]
35. Dudley, M.E.; Kolasinski, K.W. Stain etching with Fe(III), V(V) and Ce(IV) to form microporous silicon. *Electrochem. Solid State Lett.* **2009**, *12*, D22–D26. [CrossRef]
36. van den Boom, A.F.J.; Pujari, S.P.; Bannani, F.; Driss, H.; Zuilhof, H. Fast room-temperature functionalization of silicon nanoparticles using alkyl silanols. *Faraday Discuss.* **2020**, *222*, 82–94. [CrossRef] [PubMed]
37. Pujari, S.P.; Driss, H.; Bannani, F.; van Lagen, B.; Zuilhof, H. One-Pot Gram-Scale Synthesis of Hydrogen-Terminated Silicon Nanoparticles. *Chem. Mater.* **2018**, *30*, 6503–6512. [CrossRef] [PubMed]
38. Linford, M.R.; Chidsey, C.E.D. Alkyl monolayers covalently bonded to silicon surfaces. *J. Am. Chem. Soc.* **1993**, *115*, 12631–12632. [CrossRef]
39. Kolasinski, K.W. Photochemical and nonthermal chemical modification of porous silicon. In *Porous Silicon for Biomedical Applications*; Santos, H., Ed.; Woodhead Publishing (Elsevier): Duxford, UK, 2021; pp. 51–112.

40. Gräf, D.; Grundner, M.; Schulz, R.; Muhlhoff, L. Oxidation of HF-Treated Si Wafer Surfaces in Air. *J. Appl. Phys.* **1990**, *68*, 5155–5161. [CrossRef]
41. Gräf, D.; Grundner, M.; Schulz, R. Reaction of Water with Hydrofluoric-Acid Treated Silicon(111) and (100) Surfaces. *J. Vac. Sci. Technol. A* **1989**, *7*, 808–813. [CrossRef]